

A Molecular Kinetic Model incorporating Catalyst Acidity for Hydrocarbon Catalytic Cracking

Zhengyu Chen¹, Wenjin Lyu¹, Ruipu Wang¹, Yuming Li¹, Chunming Xu¹, Guiyuan Jiang¹, and Linzhou Zhang¹

¹China University of Petroleum Beijing

October 31, 2022

Abstract

We built a molecular-level kinetic model for hydrocarbon catalytic cracking, incorporating the catalyst acidity as the parameter to estimate the reaction rates. The n-decane and 1-hexene co-conversion catalytic cracking process was chosen as the studying case. The reaction network was automatically generated with a computer-aided algorithm. A modified linear free energy relationship was proposed to estimate the activation energy in a complex reaction system. The kinetic parameters were initially regressed from the experimental data under various reaction conditions. On this basis, the product composition was evaluated for three catalytic cracking catalysts with different Si/Al. The Bronsted acid and Lewis acid as the key catalyst properties were correlated with the kinetic parameters. The built model can calculate the product distribution, and molecular composition at different reaction conditions for different catalysts. The sensitive study shows that it will facilitate the model-based optimization of catalysts and reaction conditions according to product demands.

A Molecular Kinetic Model incorporating Catalyst Acidity for Hydrocarbon Catalytic Cracking

Zhengyu Chen[#], Wenjin Lyu[#], Ruipu Wang, Yuming Li, Chunming Xu, Guiyuan Jiang^{*} and Linzhou Zhang^{*}

State Key Laboratory of Heavy Oil Processing, Petroleum Molecular Engineering Center (PMEC), China University of Petroleum, Beijing, 102249, P. R. China

Abstract

We built a molecular-level kinetic model for hydrocarbon catalytic cracking, incorporating the catalyst acidity as the parameter to estimate the reaction rates. The n-decane and 1-hexene co-conversion catalytic cracking process was chosen as the studying case. The reaction network was automatically generated with a computer-aided algorithm. A modified linear free energy relationship was proposed to estimate the activation energy in a complex reaction system. The kinetic parameters were initially regressed from the experimental data under various reaction conditions. On this basis, the product composition was evaluated for three catalytic cracking catalysts with different Si/Al. The Bronsted acid and Lewis acid as the key catalyst properties were correlated with the kinetic parameters. The built model can calculate the product distribution, and molecular composition at different reaction conditions for different catalysts. The sensitive study shows that it will facilitate the model-based optimization of catalysts and reaction conditions according to product demands.

Keywords: catalytic cracking, kinetic model, catalyst acidity, catalyst design

1. Introduction

Currently, gasoline still plays a crucial part in the worldwide energy system. Fluid catalytic cracking (FCC) technology is a widely applied process for producing gasoline in modern refineries. The FCC gasoline is the main blending component for China's gasoline production.¹ However, with the increasingly stringent environmental regulations, the blending of FCC gasoline becomes a challenge to meet national gasoline quality standards.² The gasoline standard for motor vehicles worldwide severely limits the olefin content and 50 v% distillation temperatures (T_{50}) of the gasoline. To match the environmental regulation, some new technologies were proposed to produce high-quality gasoline.³ In addition to the progress of processes and equipment, cutting-edge modeling techniques also provide critical support for the development of novel technologies.^{4,5}

The petroleum refining process is a complex system involving a large number of substances and chemical reactions.⁶ To capture the detailed conversion pathways of each substance in the reaction system, researchers proposed petroleum molecular composition modeling and molecular-level kinetic modeling. To date, a variety of modeling frameworks for molecular-level kinetic modeling have been built.⁷ For example, Klein's research group has built the Kinetic Modeler's Toolkit (KMT) based on the bond-electron matrix (BEM).^{8,9} A series of molecular-level kinetic models for petroleum refining processes, such as catalytic reforming, hydrotreating, and thermal cracking, have been built based on the KMT.¹⁰⁻¹³ Froment's research group proposed a single-event kinetic model,¹⁴ and it has wide-ranging applications in catalytic reaction systems such as hydrocracking, FCC, and methanol-to-olefin

(MTO).¹⁵⁻¹⁷ Moreover, Green and his co-workers developed the Reaction Mechanism Generator (RMG).¹⁸ Van Geem et al. built a detailed kinetic model for n-hexane steam cracking using the RMG.¹⁹ The above three frameworks are primarily based on reaction mechanisms and can build the kinetic model at the mechanistic level containing reaction intermediates. For another thing, Quann and Jaffe proposed structure-oriented lumping (SOL).^{20,21} SOL can describe the chemical reactions in terms of molecular groups, and the molecular-level kinetic model based on the pathway level can be developed.²² This framework has received extensive attention and applications in petroleum process modeling.²³⁻²⁵ Further, Peng proposed the molecular type and homologous series (MTHS) matrix to construct molecular-level kinetic models by defining virtual molecules.²⁶ Recently, Zhang's research group proposed a structural unit and bond-electron matrix (SU-BEM) framework,^{27,28} and a range of molecular-level process models were built in terms of the SU-BEM framework.²⁹⁻³¹

Compared with the traditional lumped kinetic model,³²⁻³⁵ molecular-level kinetic models can calculate more physicochemical information about reactants and products. It can be used as a tool to provide necessary fundamental data for process design and optimization.⁵ At present, the FCC naphtha reformulated technologies can be divided into two categories: one is the direct upgrade of the conventional FCC riser, represented by the maximizing iso-paraffins (MIP) technology. The MIP process can significantly reduce the olefin content in gasoline by using a diameter expanding riser. Qin et al. built a heavy oil FCC kinetic model at the molecular level for the MIP process. The model adopted the SOL framework, and the gasoline quality of MIP and conventional FCC technology were compared in detail.³⁶ Another is the individual reformulation for the FCC naphtha. Chen et al. used the SU-BEM framework to simulate the

FCC naphtha olefin reduction process at the molecular level. The results indicated that a large number of olefin molecules were converted to iso-paraffins and aromatics with higher octane number during the naphtha reformulation process.³⁷

Previous studies have shown that molecular-level kinetic models can predict product variations with reacting conditions. However, high-efficiency catalytic materials have a more significant impact on product distribution and properties in industrial-scale practice.³⁸ In addition, the design and screening of suitable catalysts also facilitate the accelerated research and development (R & D) of novel processes. Xiong et al. selected a series of FCC catalysts and correlated the kinetic parameters in the six-lumped model with the catalyst properties.³⁹ The built model accurately calculated the lumped yields under different catalysts. Presently, the published work focuses on the correlation between catalyst properties and parameters of the lumped models, and some semi-empirical or quantitative correlation models were reported.⁴⁰⁻⁴² However, there were few studies for building molecular-level reaction kinetic models incorporating catalyst properties.⁴³

In this work, a molecular-level kinetic model of catalytic cracking was developed for a novel head-tail co-conversion process for gasoline fraction proposed by Wang et al.⁴⁴. Three commercial catalysts were selected, and the hydrocarbon catalytic cracking experiments were carried out by using these catalysts, respectively. Obtained experimental data was used to build the kinetic model containing the catalyst acidity. An excellent agreement was observed between experimental and predicted values. The developed model demonstrates that the molecular-level reaction kinetic model can be quantitatively correlated with catalyst acidity. It will facilitate the design and screening of catalysts and expand the application scenarios of molecular-level

kinetic models.

2. The head-tail co-conversion process

The head-tail co-conversion process is a novel gasoline fraction reformulation process proposed by Wang et al.⁴⁴. We performed a detailed molecular composition analysis of naphtha from different FCC units and found that the carbon number of olefins is mainly between 5 and 7. Furthermore, the n-paraffins with carbon numbers from 10 to 12 have a relatively high boiling point, and they negatively contribute to both the octane number and T₅₀ of gasoline. Interestingly, the C-C bond dissociation energy of these molecules (C5~7 olefins are 310-315 kJ/mol, and C10~12 n-paraffins are 355-360 kJ/mol) are similar.⁴⁵ If they can be converted together into gaseous components using catalytic cracking technology, the olefins and T₅₀ in gasoline can be reduced simultaneously. Thus, in this work, 1-hexene and n-decane were selected as the feedstock for moderate catalytic cracking to obtain the basic experimental data. The detailed experimental flowsheet and process conditions are shown in Figure 1.

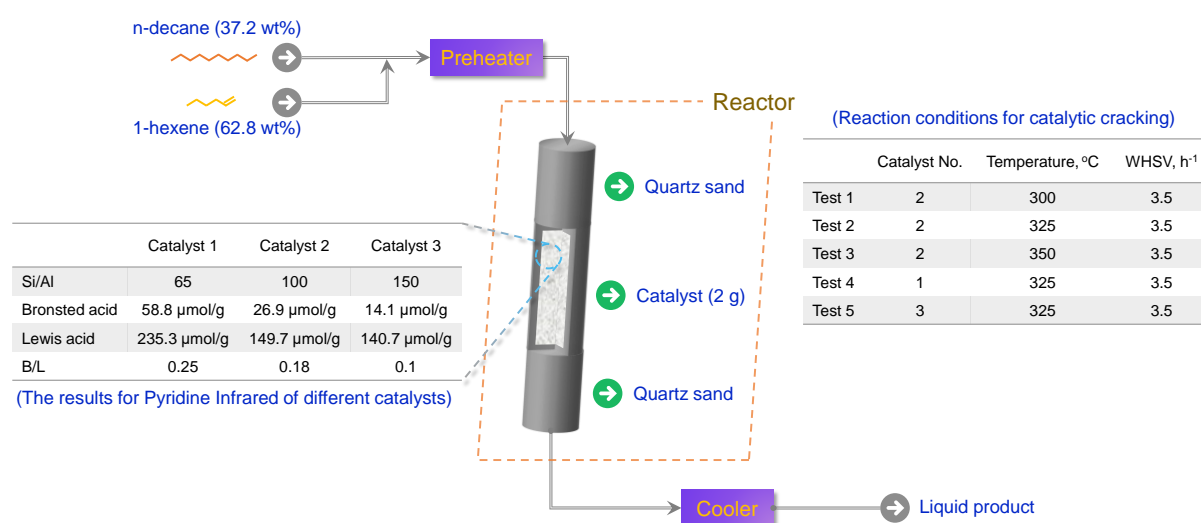


Figure 1. Experimental device and process condition for hydrocarbon catalytic cracking

The feedstock was a mixture of n-decane and 1-hexene (1:1, mol/mol). The feedstock was pumped into the preheater and heated to the reaction temperature. The reactor was a fixed bed reactor filled with 2 g of commercial catalytic cracking catalyst. According to the Si/Al, three commercial HZSM-5 catalysts were selected. The Bronsted acid (B acid) and Lewis acid (L acid) of three catalysts were obtained by pyridine infrared, as shown in Figure 1. The preheated feedstock was delivered into the reactor, and the catalytic cracking occurred. The investigation of process conditions was discussed in detail in the previous work.⁴⁴ In this work, process conditions were set with reference to previous experiments, as shown in Figure 1. The obtained product molecules were cooled and sent to gas chromatography (GC) to determine the molecular composition.

According to the above experimental procedure and reaction conditions, a molecular-level kinetic model for n-decane and 1-hexene catalytic cracking was constructed. The model parameters were firstly tuned by the experimental data from tests 1~3. It can eliminate the effect of the catalyst. On this basis, the catalyst factor was introduced and correlated with the kinetic model. The B acid and L acid of the catalyst were selected as the key properties in the catalyst factor. Subsequently, the catalyst parameters would be tuned using the data from tests 2, 4, and 5. The corresponding catalyst number are catalysts 2, 1, and 3. The constructed model can calculate the gasoline yield and composition under various reaction conditions and acid contents.

3. Molecular-Level Kinetic Model

3.1 Reaction rule and reaction network

This work applied the SU-BEM framework to develop the molecular-level kinetic model for hydrocarbon catalytic cracking.²⁸ The framework employs group conversions to describe chemical reactions. The large-scale reactions can be generated automatically by performing a range of reaction rules.

According to the reaction mechanism of carbonium ions and the product molecular composition,⁴⁶ we deduced and programmed 23 reaction rules for gasoline fraction catalytic cracking, as listed in Figure 2. Three typical reactions (n-decane cracking, 1-hexene isomerization, and benzene alkylation) were selected to exhibit further the programmed process of reaction rules based on structural unit changes. We take the n-decane cracking reaction as an example. First, the structural unit of n-decane ('R=10;') in the feedstock needs to be screened out through the reactant selection rule. Subsequently, the structural units of the reactants are modified according to the product generation rule, and the product molecules ('R=5;' and 'R=5; RIH=-2; ') can be obtained. According to the above steps, the corresponding chemical reaction can be available. In addition to the above examples, the reaction rules also covered the cracking, dehydrogenation, and isomerization of paraffins, the cracking, cyclization, isomerization, polymerization, and alkylation of olefins. For the naphthenes and aromatics, dehydrogenation, ring opening, hydrogen transfer, and dealkylation were also considered. More details on the reaction rules can be available in our previously published work.^{28,37}

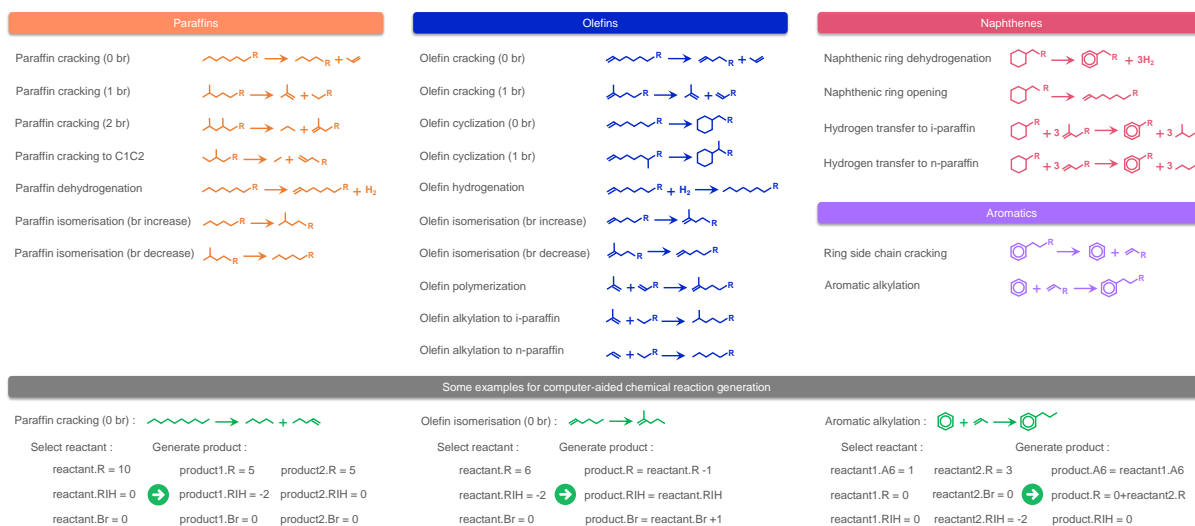


Figure 2. Reaction rules for the catalytic cracking.

After determining the reaction rules, we input the structural units of n-decane and 1-hexene into the 23 reaction rules. An in-house reaction network auto-generation algorithm was used, and the reaction network for n-decane and 1-hexene catalytic cracking was obtained. There are 74 molecules and 469 reactions in this network, and the topological graph for the whole reaction network was shown in Figure 3(b). The partial reaction network for the catalytic cracking is displayed in Figure 3(a). The colors of the lines in the figure represent the different reaction rules, and it can visually reveal the conversion relationship between individual molecules. The n-decane can be converted by the isomerization reaction and can also undergo the cracking reaction to generate the low-carbon paraffins and olefins. For the olefin, such as 1-hexene, they can continue to be cracked into light olefins, such as propylene, butene, and other high value-added products. Moreover, Olefins can also undergo the cyclization reaction to generate the naphthenes. The formed naphthenes further undergo hydrogen transfer with olefins, and the aromatics and paraffins can be obtained.

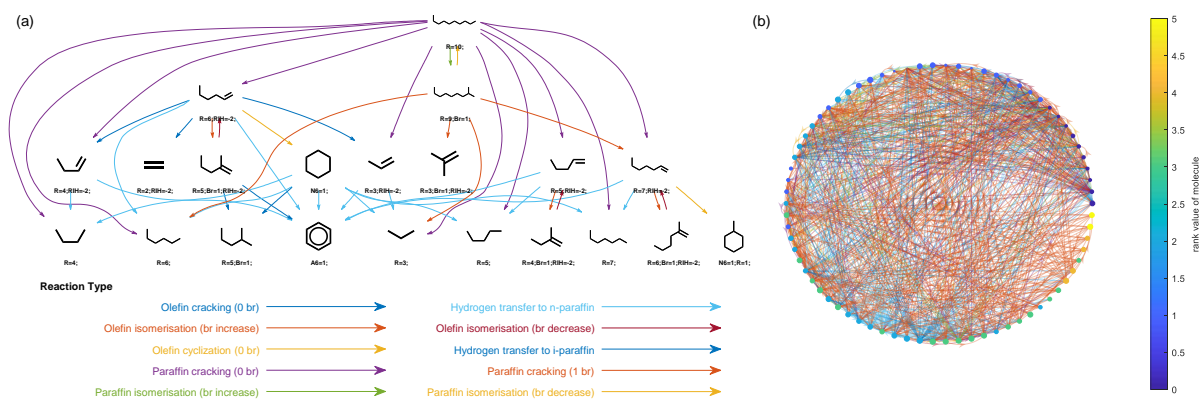


Figure 3. Visualization of the reaction network for n-decane and 1-hexene catalytic cracking. (a) The partial reaction network for molecular conversion; (b) Topological graph for the whole reaction network.

3.2 Kinetic model

To develop the kinetic model, we converted the reaction network into the reaction rate equation by a piece of in-house code. The hydrocarbon catalytic cracking belongs to the gas-solid non-homogeneous reaction system, and the Langmuir-Hinshelwood-Hougen-Watson (LHHW) model was selected as the kinetic model, as shown in Eq. (1) and (2). Then, the LHHW was substituted into the reaction rate equation, and the ODE (ordinary differential equation) solver was called to compute the product molecular distribution.

$$r_j = \frac{k_{srj} K_{adsA} K_{adsB} (C_A^m C_B^n)}{1 + \sum K_{adsi} C_i} \quad (1)$$

$$k_{srj} = A_j e^{-\frac{E_{aj}}{RT}} \quad (2)$$

For the complex reaction system, linear free energy relationship (LFER) was commonly used to estimate the activation energy of each reaction.⁴⁷ LFER correlates the reaction enthalpy with the activation energy. It is assumed that the reaction enthalpy is linearly related to the activation energy for the same type of chemical reaction^{48,49}. Accordingly, the activation energy

of each reaction can be calculated from the reaction enthalpy, as shown in Eq. (3) and (4). Eq. (3) is for the exothermic reaction, while Eq. (4) is for the endothermic reaction.

$$Ea_j = E_{0_n} - \alpha_n \times \Delta H_j \quad (3)$$

$$Ea_j = E_{0_n} - (1 - \alpha_n) \times \Delta H_j \quad (4)$$

The LFER was frequently applied in the reaction system of middle distillates or heavy oil. However, a recent study has shown that the LFER is insufficient calculation accuracy for the light fraction (such as gasoline fraction) conversion process.³⁷ It is mainly due to the relatively simple molecular composition of the light fraction, leading to requiring the model to calculate more product details. Besides the distribution and composition of the product, it is also necessary to calculate the carbon number distribution and even the content of critical molecules. The excessive details caused the reactions in the model not strictly to obey the LFER, resulting in poor model accuracy. To overcome this limitation, we modified the LFER and introduced the reactivity index based on the original equations. The modified LFER was shown in Eq. (5) and (6).

$$Ea_j = E_{0_n} - \alpha_n \times \Delta H_j + \beta_n RI^{\gamma_n} \quad (5)$$

$$Ea_j = E_{0_n} - (1 - \alpha_n) \times \Delta H_j + RI^{\gamma_n} \quad (6)$$

RI represents the reactivity index. It is mainly used to reflect the influence of the physicochemical properties of the reactants or products on the activation energy.⁵⁰ The index can be the molecular structure parameter, such as the carbon number, number of rings, and number of branched chains. For example, for the n-paraffins cracking reaction, the C-C bond energy at various positions is different. In general, carbon-carbon bonds near the middle are more likely to break. However, the traditional LFER hardly reflects this phenomenon. Therefore, we can set the RI as the carbon number ratio of two products based on this

phenomenon. After incorporating the structural information of the molecule, the model can estimate the activation energy of each reaction more accurately. Furthermore, for the adsorption constant in the LHHW, the classical quantitative structure-reactivity correlations (QSRCs) are adopted in this work,^{51,52} and the adsorption constant was correlated by the molecular structure, as shown in Eq. (7).

$$\ln K_{ads_i} = a + \frac{(bN_{AR_i} + cN_{SC_i})}{RT} \quad (7)$$

3.3 Parameter regression

To calculate the product distribution and gasoline composition, this work regressed the model parameters by the experimental data from various process conditions. The absolute error between experimental measurement and calculated value was taken as the objective function. The gasoline yield and composition were delivered into the model, and the genetic algorithm (GA) was applied to tune the preexponential factor and the parameters in the modified LFER. A comparison between experimental and calculated data is displayed in Figure 4. The optimized parameters are listed in Table 1. The results indicate that the calculated data of product distribution and composition agree well with the experimental measurement under the various reaction conditions.

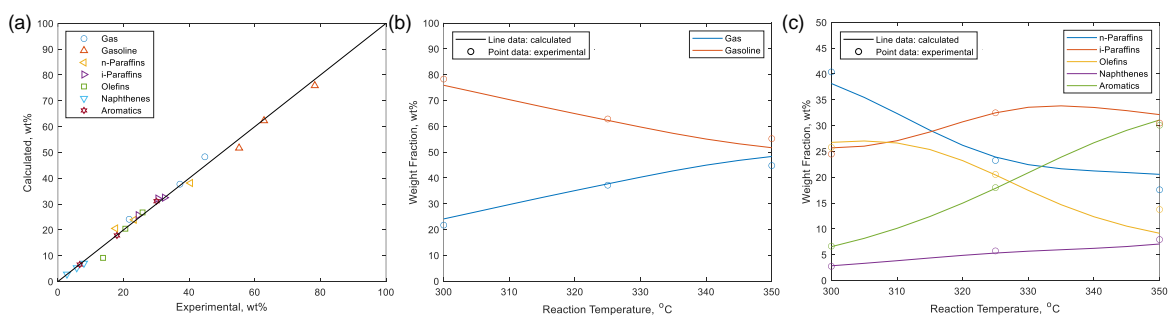


Figure 4. Comparison between experimental and calculated values for different process conditions. (a) parity plot; (b) fraction yield; (c) gasoline composition.

Table 1. Modified LFER parameters in the catalytic cracking model

Reaction family	modified LFER parameters				
	α	E_0	RI^a	β	γ
Aromatic alkylation	300	15000	R_n	0	1
Hydrogen transfer to i-paraffin	2500	-336000	R_n	-5000	1
Hydrogen transfer to n-paraffin	3500	-470000	R_n	-6000	1
Naphthenic ring dehydrogenation	-6849	1409617	R_n	0	1
Naphthenic ring opening	75.3	4069	R_n	0	1
Olefin alkylation to i-paraffin	15	10549.8	P_n	1	3.51
Olefin alkylation to n-paraffin	20	-1667	P_n	330	2
Olefin cracking (0 br)	100	96665	R_n	0	1
Olefin cracking (1 br)	1280	-1726	R_n	0	1
Olefin cyclization (0 br)	-100	202900	R_n	0	1
Olefin cyclization (1 br)	213	79971.9	R_n	0	1
Olefin hydrogenation	79	17316.5	R_n	0	1
Olefin isomerisation (br increase)	522	5695.4	R_n	0	1
Olefin isomerisation (br decrease)	325	17319.8	R_n	0	1
Olefin polymerization	156	-13002.7	R_{1n}/R_{2n}	21000	1.2
Paraffin cracking (0 br)	1766.4	-8335.1	P_{2n}/P_{1n}	2775	1.07
Paraffin cracking (1 br)	2424	102900	R_n	0	1
Paraffin cracking (2 br)	99	82036	R_n	0	1
Paraffin cracking to C1C2	-2000.3	105000	$1/R_n$	2889000	1
Paraffin dehydrogenation	235	56554.6	R_n	0	1
Paraffin isomerisation (br increase)	1000	-8246.5	$1/R_n$	21890	0.15
Paraffin isomerisation (br decrease)	1500	-32369.8	$1/R_n$	965445.4	1
Ring side chain cracking	300	65000	R_n	0	1

a. Reactivity index for the reactant or product

b. R_n : Carbon number for the reactant, R_{1n} : Carbon number for reactant 1, R_{2n} : Carbon number for reactant

2 ($R_{2n} \geq R_{1n}$).

c. P_n : Carbon number for the product, P_{1n} : Carbon number for product 1, P_{2n} : Carbon number for product 2

($P_{2n} \geq P_{1n}$).

Moreover, to further investigate the robustness of the model, we explored the influence of reaction temperature on the yield and composition of the gasoline fraction, as shown in Figures 4(b) and (c). The results demonstrate that the built model can accurately capture the transformation behavior of the n-decane and 1-hexene catalytic cracking. With the growth of reaction temperature, the rate of cracking reaction rate is accelerated. More feedstock molecules undergo cracking reactions to produce the gaseous substance, leading to a decrease in the gasoline fraction. For the gasoline composition, reaction rates of cyclization and dehydrogenation speed up when the reaction temperature rises. It resulted in an increased yield for naphthenes and aromatics. Due to the accelerated cracking reaction, the yields of olefins and n-paraffins gradually reduce. When the reaction temperature is 325 °C, the olefin content in the gasoline drops to around 20 wt%. The results demonstrate that the novel head-tail co-conversion technology can effectively reduce the olefin content. Meanwhile, n-paraffins, which have a negative contribution to the octane number, are also efficiently converted. For high-quality gasoline, iso-paraffins are the ideal component for gasoline blending.⁵³ Figure 4(c) shows that the iso-paraffins first increase and then decrease. It is because the reaction rate for the cracking is relatively slow when the temperature is low. n-Paraffins and n-olefins were converted into paraffins and olefins with branches by the isomerization reaction. Isomeric olefins can also undergo hydrogen transfer to generate iso-paraffins. However, as the reaction temperature rises, the activation energy of the cracking reaction is normally higher than that of isomerization and hydrogen transfer. It means that the cracking reaction rate will increase faster than the isomerization and hydrogen transfer. The n-paraffins and olefins in the feedstock are preferred for cracking to light olefins. Moreover, the generation rate of iso-paraffins is also less

than the consumption rate under high temperature conditions, leading to a decrease in the iso-paraffin content.

Compared with the kinetic model at the lumped level, the molecular-level kinetic model can obtain more detailed information about the reaction system, such as carbon number distribution and molecular composition. Figure 5 displays the predicted results of the detailed carbon number distribution for gasoline, in which a good agreement was observed. The reaction condition is test 2, as shown in Figure 1. In general, the carbon number of the gasoline fraction ranges from 5 to 8. n-Paraffins are mainly distributed among C5 to C7, while naphthenes and aromatics range from 7 to 9. According to the product molecular distribution, the head-tail co-conversion process can effectively convert the olefin into the iso-paraffins. Moreover, there is relatively low content for molecules with carbon numbers 9 and 10, as shown in Figure 5(f). It means that the process is beneficial in reducing the T_{50} of gasoline.

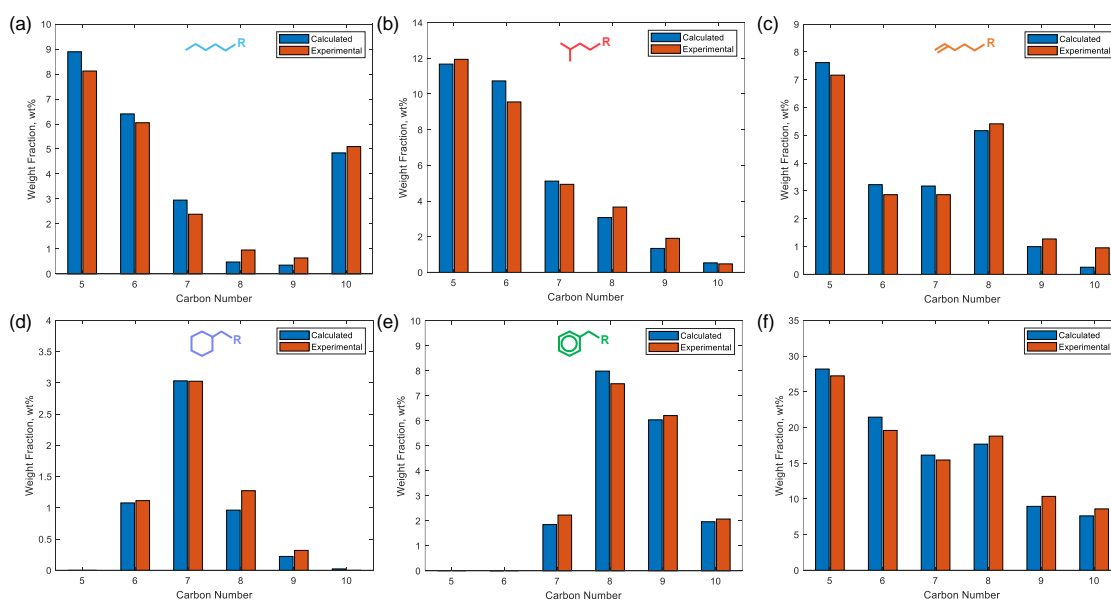


Figure 5. Comparison between experimental and predicted data for carbon number in gasoline fraction. (a) n-paraffins; (b) i-paraffins; (c) olefins; (d) naphthenes; (e) aromatics; (f) total carbon number distribution.

The tuned model has obtained the yield, composition, and carbon number distribution of the gasoline fraction. To further validate the extrapolation of the model, we used the model to predict a series of molecules with high content in the product. The comparison of experimental and predicted values is exhibited in Figure 6. It is important to note that these experimental data were not input to the optimization algorithm during the parameter regression. The results reveal that the built model can acquire the conversion pattern of key components and predict their yields. The n-decane in the feedstock is sensitive to the reaction temperature. When the temperature is raised from 300 °C to 325 °C, the unconverted n-decane decreases from 20 wt% to less than 5 wt%. It indicates that the increase in temperature dramatically improves the reaction rate for n-paraffins cracking. In addition, it can be seen from the figure that yields of some molecules with lower carbon numbers, such as C3 and C4, have a generally growing trend as the temperature rises. The phenomenon also matches with the reaction mechanism of catalytic cracking. Overall, the molecular-level kinetic model for n-decane and 1-hexene catalytic cracking can accurately compute and predict the yield, detailed carbon number distribution, and key molecular composition of the product. The model can be used as a foundation for developing a model integrating catalyst acidity.

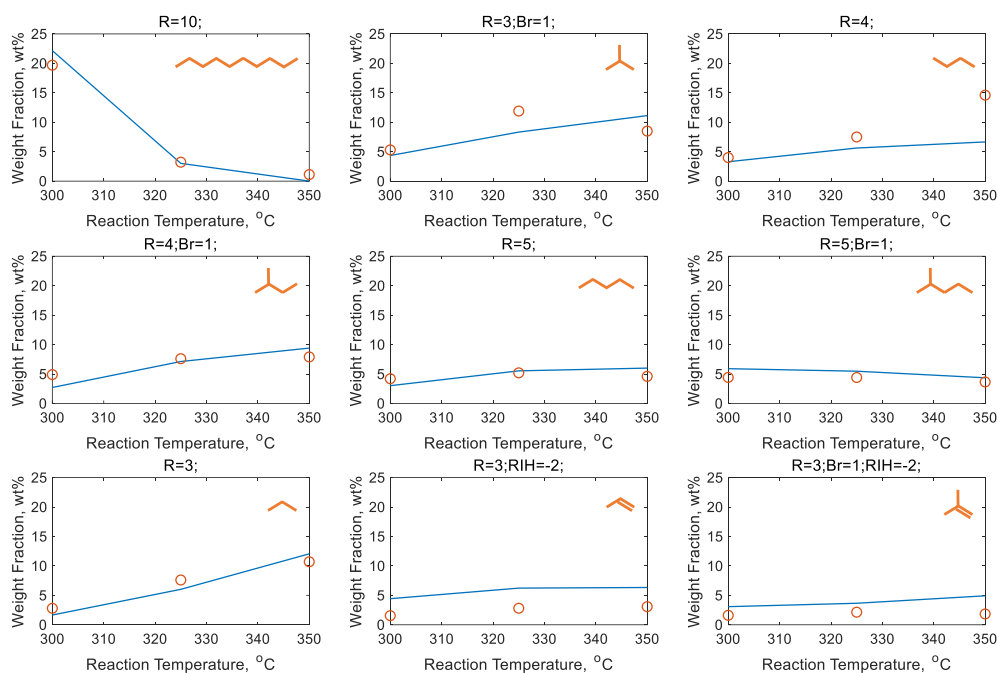


Figure 6. Comparison between experimental and predicted values for key product molecules under different reaction temperatures (Line is the predicted data, and the point is the experimental data).

4. Molecular-level kinetic model incorporating catalyst acidity

4.1 Mathematical model

Many properties in the catalyst will influence product distribution. If we correlated all the properties measured during catalyst characterization, it would be a model combined with all factors. However, in industrial practice, it is a challenging task for the refinery to obtain a full range of catalyst properties. The absence of some properties will limit the generalization and application of the model. To develop a practical model, we need to screen the key properties to be associated. Pyridine infrared is a well-known method for catalyst characterization, and it can obtain the acid type and acid content of the catalyst. The acid type and acid content are crucial factors affecting the product distribution for the catalytic cracking process.⁵⁴⁻⁵⁶ Thus,

this work selected the B acid and L acid as the critical catalyst properties, and they were correlated with the kinetic model. The proposed mathematical model was shown in Eq. (8) and (9), and Cat_a_n and Cat_b_n are the parameters to be regressed

$$k_{srj} = \varphi_n A_j e^{-\frac{Ea_j}{RT}} \quad (8)$$

$$\varphi_n = (B\ acid/26.94)^{Cat_a_n} (L\ acid/149.7)^{Cat_b_n} \quad (9)$$

4.2 Parameter regression

After the mathematical model was presented, three catalytic cracking catalysts with different Si/Al were determined. The acid type and content were obtained by the pyridine infrared, as shown in Figure 1. The results show that the B acid and L acid content gradually declined with the increase of the Si/Al. Meanwhile, the ratio of B acid to L acid also progressively reduced. After that, catalytic cracking experiments were performed using the three catalysts, respectively. The product distribution was obtained, and the catalyst parameters were also tuned. The tuned catalyst parameters are listed in Table 2, while the comparison between the experimental and calculated values is shown in Figure 7. The results show that the calculated values of the model incorporated catalyst acidity have a great agreement with the experimental measurement. The gasoline yield gradually rises as the Si/Al increases. It is mainly due to the reduced acidity of the catalyst. For gasoline composition, the reduction of Si/Al improves the naphthene and aromatic yields, while yields of n-paraffins and olefins decrease. Meanwhile, the yield of iso-paraffins, as the high-value components, also continues to increase. It also reveals that the conversion efficiency of catalytic cracking gradually grows. Moreover, when the Si/Al increased from 100 to 150, the variation of gasoline composition was significantly greater than that from 65 to 100.

Table 2. The tuned parameter for catalysts in the catalytic cracking model

Reactions family	<i>Cat_a</i>	<i>Cat_b</i>
Aromatic alkylation	-0.324	-0.076
Hydrogen transfer to i-paraffin	4.244	-7.329
Hydrogen transfer to n-paraffin	4.244	-7.329
Naphthenic ring dehydrogenation	0.747	-1.291
Naphthenic ring opening	0.170	-0.083
Olefin alkylation to i-paraffin	-0.324	-0.076
Olefin alkylation to n-paraffin	-0.324	-0.076
Olefin cracking (0 br)	1.307	-1.853
Olefin cracking (1 br)	-0.046	0.483
Olefin cyclization (0 br)	1.175	-1.133
Olefin cyclization (1 br)	1.175	-1.133
Olefin hydrogenation	0.073	0.065
Olefin isomerisation (br increase)	-0.054	0.570
Olefin isomerisation (br decrease)	-0.054	0.570
Olefin polymerization	0.622	-0.765
Paraffin cracking (0 br)	1.329	-2.084
Paraffin cracking (1 br)	1.329	-2.084
Paraffin cracking (2 br)	1.329	-2.084
Paraffin cracking to C1C2	2.110	-2.692
Paraffin dehydrogenation	0.073	0.065
Paraffin isomerisation (br increase)	-0.176	0.303
Paraffin isomerisation (br decrease)	-0.176	0.303
Ring side chain cracking	1.329	-2.084

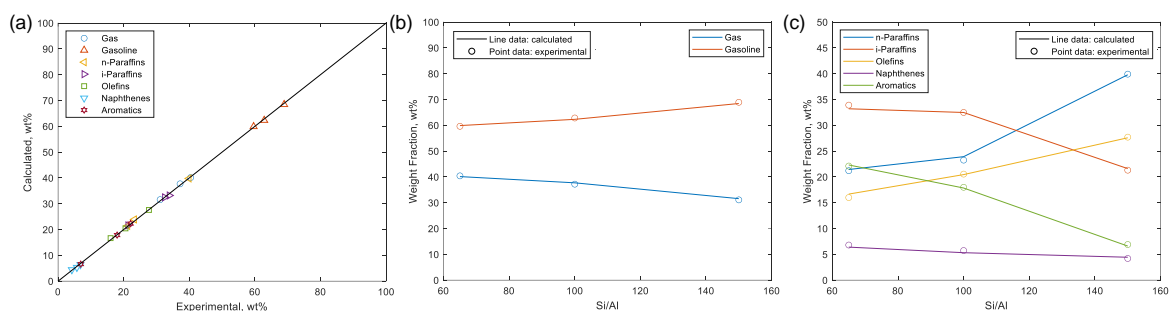


Figure 7. Comparison between experimental and calculated values for different catalysts.

4.3 Model evaluation

In addition to accurately calculating the yield and composition of the product, the model should also be able to predict the detailed carbon number distribution for gasoline fraction under various catalysts. The predicted data were compared with the experimental data, as shown in Figure 8. The predicted values agree with the experimental values as the catalyst acidity change. Except for catalyst 3, the carbon number of the gasoline derived from catalysts 1 and 2 mainly ranges from 5 to 8. For catalyst 3, the conversion efficiency is obviously insufficient, and a large number of n-decane in the feedstock is still unconverted. The product distribution of catalysts 1 and 2 is relatively similar in terms of molecular type. The content for C5 and C6 in paraffins is relatively high. For the olefin, C5 is the most abundant, and C6 olefins are efficiently converted. The carbon number of naphthenes and aromatics is distributed from 7 to 9. For catalyst 3, the unconverted n-decane dominate, and the distribution of iso-paraffin presents the gamma distribution. Naphthenes and aromatics also range from C7 to C9. In addition to the high content of C5 olefins, olefin molecules with carbon numbers from 6 to 8 are relatively average. According to the product carbon number distribution, catalysts 1 and 2 are well suited to match the production purpose of the head-tail co-conversion process. However, compared to catalyst 1, catalyst 2 is beneficial for retaining more components in the gasoline fraction.

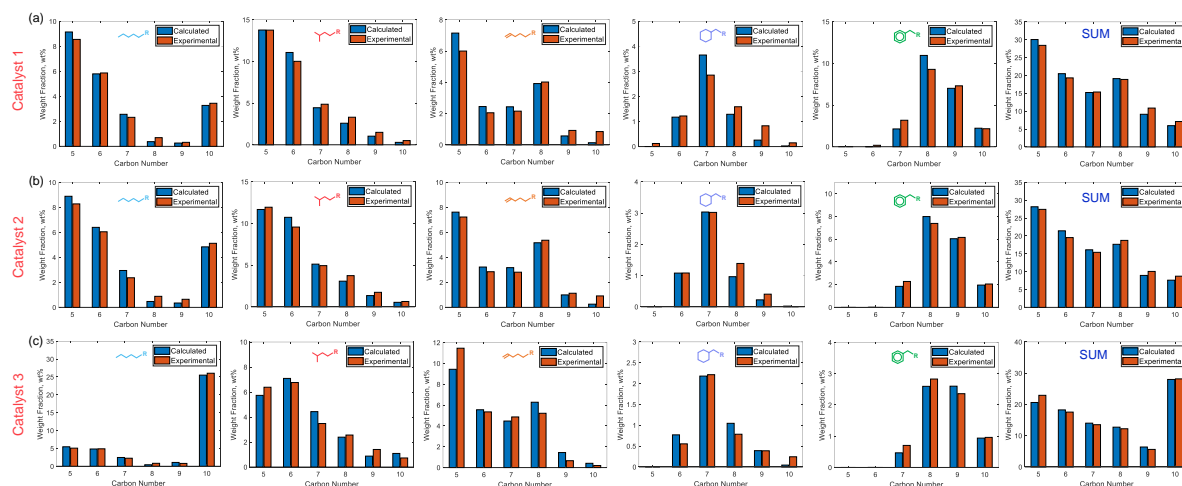


Figure 8. Comparison between predicted and experimental values for carbon number in gasoline fraction. (a) catalyst 1, (b) catalyst 2, (c) catalyst 3.

In addition to the detailed carbon number distribution, the key component content was also predicted, as shown in Figure 9. The results show that the distribution of each molecule is in agreement with the experimental values, and the predictive capability of the model was re-validated. As the Si/Al increases, the acid content of the catalyst decreases. The reaction rate of the cracking drops, resulting in the yields of the gaseous component reducing. For the n-decane, when the Si/Al varies from 100 to 150, the conversion rate of the n-decane declined remarkably. The content of the n-decane is 4 wt% and 19 wt%, respectively. It reflects that the conversion efficiency of the catalytic cracking reduces.

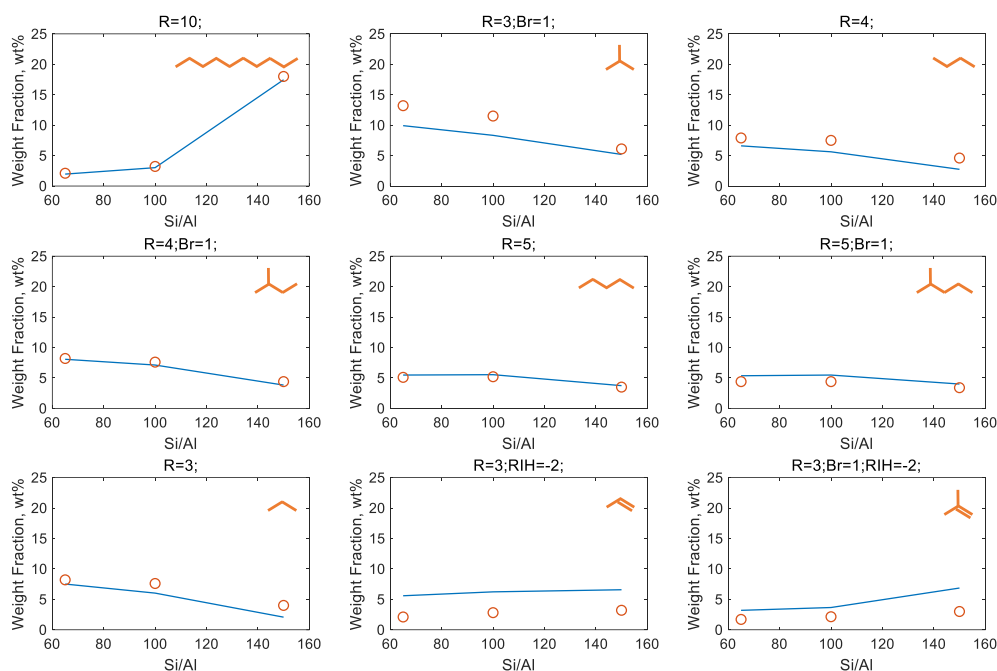


Figure 9. Comparison between experimental and calculated values for key product molecules under different catalysts (Line is the predicted data, and the point is the experimental data).

We have compared the product distribution at the reactor outlet and demonstrated that the model incorporating catalyst acidity could accurately calculate and predict the distribution and composition of the product. Subsequently, the reaction processes for n-decane and 1-hexene catalytic cracking are further predicted when catalysts vary, as shown in Figure 10. Figure 10 exhibits the distribution of product yield, gasoline composition, and gasoline carbon number along the fixed bed reactor. As can be seen from the figure, in the first 40 % of the reactor, the cracking reaction occurs rapidly, and a large number of gaseous components are generated. While the subsequent reactions are more moderate, the feedstock is progressively converted. For the gasoline composition, the head-tail co-conversion process mainly consumes n-paraffins and olefins to produce iso-paraffins, naphthenes, and aromatics. The formation rate of iso-

paraffins is the fastest. In the preliminary stage of the reaction, the formation rate of naphthenes is also relatively fast. However, as the naphthene yield increases, the reaction rate of dehydrogenation and hydrogen transfer accelerates. A large number of naphthenes and olefins were converted into aromatics and iso-paraffins. For the carbon number distribution in the gasoline fraction, as catalytic cracking proceeds, the molecules with carbon numbers 6 and 10 are reduced. Furthermore, the results show that the C10 molecules can be converted effectively for catalysts 1 and 2. Overall, Figure 10 displays the conversion pattern of n-decane and 1-hexene catalytic cracking at three levels: fraction, composition, and carbon number distribution.

It will be helpful to guide the design and screening of catalysts based on the target product.

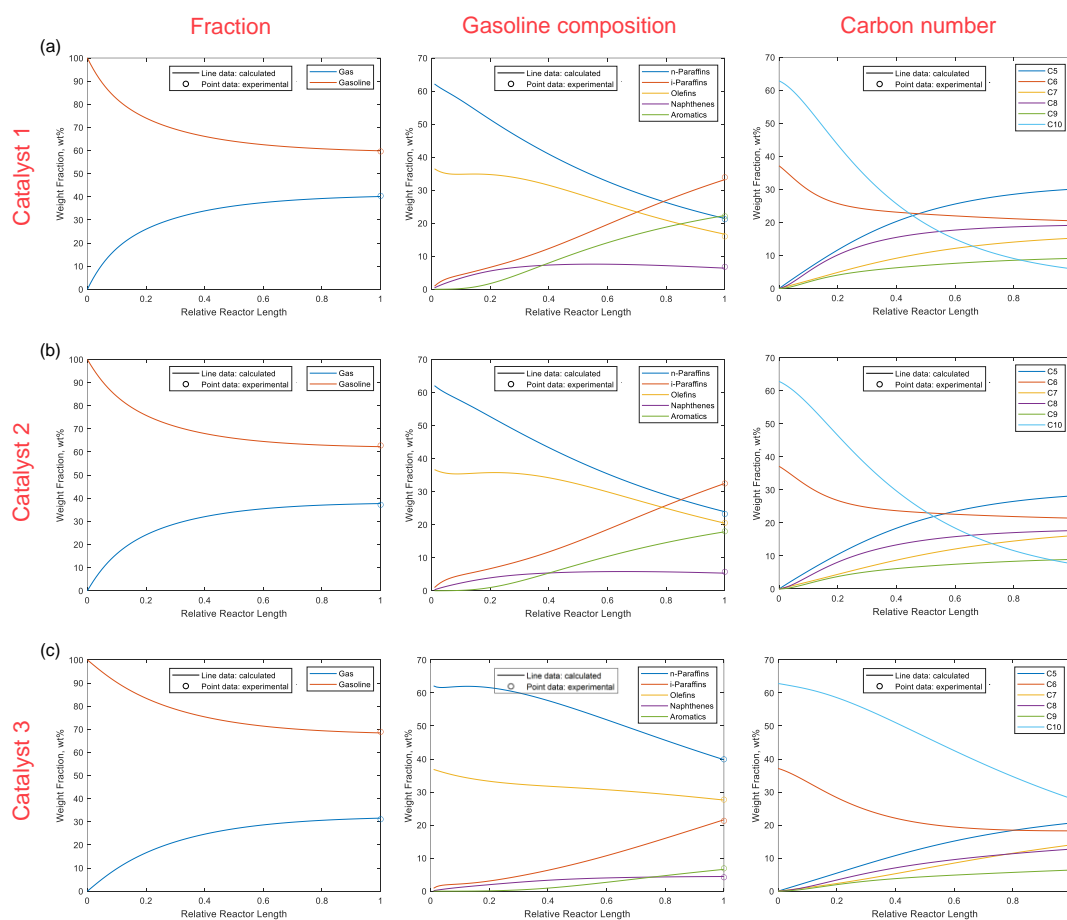


Figure 10. The distribution of the product along the reactor. (a) catalyst 1; (b) catalyst 2; (c) catalyst 3.

To further explore the effect of catalyst acidity on reaction results, we performed a sensitivity analysis to the model, as shown in Figure 11. The results indicate that the gasoline yield gradually drops as the B acid content increases. It is mainly because that B acid prefers C-C bond breaking, while L acid preferentially promotes the cleavage of the C-H bond.^{57,58} With the increase of L acid, the contact probability of reactants with B acid relatively decreases, leading to a lower conversion rate. Moreover, the growth of L acid tends to raise the olefin content in gasoline. The results in Figure 11(c) exhibit that there is a maximum value of olefin yield. When L acid content is high and B acid content is low, it can reduce the feedstock conversion rate and olefin yield, but the yield of iso-paraffins is too low. The product composition is not high-quality gasoline. Iso-paraffins are critical components of gasoline. If we intend to obtain more iso-paraffins, the selected catalyst needs to maintain a relatively high B and L acid. However, an excessive acid content tends to aggravate cracking and dehydrogenation reactions, resulting in lower gasoline and iso-paraffin yield. Therefore, according to the production purpose of the head-tail co-conversion process, A catalyst with moderate B acid and L acid is recommended. It is beneficial to obtain more gasoline fractions while reducing olefins.

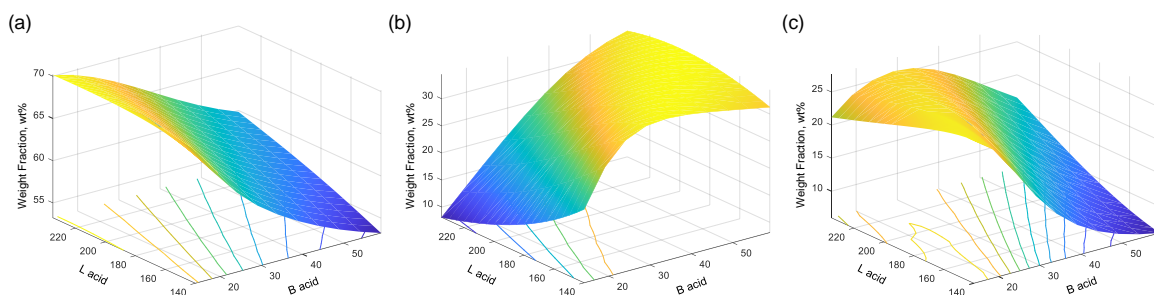


Figure 11. The effect of catalyst acidity on the gasoline yield and composition. (a) gasoline yield. (b) i-paraffins in the gasoline. (c) olefins in the gasoline.

6. Conclusion

This work developed a novel method for coupling the catalyst acidity with the molecular-level kinetic model. A molecular kinetic model for the n-decane and 1-hexene catalytic cracking was built according to the SU-BEM framework. A catalytic cracking reaction network containing 75 molecules and 469 reactions was generated in terms of the carbonium ion reaction mechanism. To improve the predictive power of the model, we modified the traditional LFER. The modified LFER can combine with the structural parameter of the molecules. The results show that the calculated values of the fraction, composition, and molecular distribution agree well with experimental values by using the modified LFER. Subsequently, we selected three HZSM-5 catalysts with different Si/Al. The product distribution for catalytic cracking was also obtained by using these catalysts. On this basis, the B acid and L acid contents were correlated with kinetic parameters, and a model incorporating catalyst acidity was proposed. The results show that the constructed model can accurately calculate and predict the carbon number distribution, composition, and yield of the gasoline fraction. It further validates the reliability of the method. The proposed method facilitates efficient design and screening of catalysts in terms of production purposes and also expands the application scenarios of molecular-level kinetic models.

Nomenclature

a, b, c = Adsorption parameters

A_j = Arrhenius constant of reaction j

E_{a_j} = Activation energy of reaction j , kJ

E_{0_n} = Activation energy factor in the LFER of reaction family n , kJ

Cat_{a_n}, Cat_{b_n} = Catalyst property parameters for reaction family n

C_i = Concentrations of species i , kmol/m³

k_{sr_j} = Surface reaction rate constant of reaction j

K_{ads_i} = Adsorption constant of species i

m = Stoichiometry of reactant A

n = Stoichiometry of reactant B

r_j = Reaction rate of reaction j

R = Universal gas constant, J/mol·K

RI = Reactivity index

T = Reaction temperature, K

ΔH_j = Enthalpy for reaction j , kJ/kmol

α_n = Reaction index factor in the Bell-Evans-Polyani LFER of reaction family n

β_n = Reactivity index factor in the modified LFER of reaction family n

γ_n = Reactivity index factor in the modified LFER of reaction family n

φ_n = Catalyst factor for reaction family n

Author Information

The first two authors (Z. Chen and W. Lyu) contribute equally to this work.

*Corresponding Author Email: jianggy@cup.edu.cn (G. Jiang) and Lzz@cup.edu.cn (L. Zhang)

Acknowledgments

This work was supported by National Natural Science Foundation of China (Nos. 22222815, 22225807). The authors declare no competing financial interests.

Reference

1. Shi Q, Zhao S, Zhou Y, Gao J, Xu C. Development of heavy oil upgrading technologies in China. *Reviews in Chemical Engineering*.2020;36(1):1-19.
2. Ivanchina ED, Kirgina MV, Chekantsev NV, Sakhnevich BV, Sviridova EV, Romanovskiy RV. Complex modeling system for optimization of compounding process in gasoline pool to produce high-octane finished gasoline fuel. *Chemical Engineering Journal*.2015;282:194-205.
3. Velázquez HD, Cerón-Camacho R, Mosqueira-Mondragón ML, et al. Recent progress on catalyst technologies for high quality gasoline production. *Catalysis Reviews*.2022:1-221.
4. Zhou X, Yang Q, Yang S, et al. One-step leap in achieving oil-to-chemicals by using a two-stage riser reactor: Molecular-level process model and multi-objective optimization strategy. *Chemical Engineering Journal*.2022;444:136684.
5. Zhu FXX, Xu L. Integrating multiscale modeling and optimization for sustainable process development. *Chemical Engineering Science*.2022;254:117619.
6. Chen Z, Guan D, Zhang X, et al. A mass-temperature decoupled discretization strategy for large-scale molecular-level kinetic model. *Chemical Engineering Science*.2022;249:117348.
7. Ali SA, Alshareef AH, Theravalappil R, Alasiri HS, Hossain MM. Molecular Kinetic Modeling of Catalytic Naphtha Reforming: A Review of Complexities and Solutions. *Catalysis Reviews*.2022:1-54.
8. Wei W, Bennett CA, Tanaka R, Hou G, Klein MT, Klein MT. Computer aided kinetic modeling with KMT and KME. *Fuel Processing Technology*.2008;89(4):350-363.

9. Broadbelt LJ, Stark SM, Klein MT. Computer Generated Pyrolysis Modeling: On-the-Fly Generation of Species, Reactions, and Rates. *Industrial & Engineering Chemistry Research*.1994;33(4):790-799.
10. Nguyen TT, Teratani S, Tanaka R, Endo A, Hirao M. Development of a structure-based lumping kinetic model for light gas oil hydrodesulfurization. *Energy & Fuels*.2017;31(5):5673-5681.
11. Wei W, Bennett CA, Tanaka R, Hou G, Klein MT. Detailed kinetic models for catalytic reforming. *Fuel Processing Technology*.2008;89(4):344-349.
12. Horton SR, Zhang L, Hou Z, Bennett CA, Klein MT, Zhao S. Molecular-Level Kinetic Modeling of Resid Pyrolysis. *Industrial & Engineering Chemistry Research*.2015;54(16):4226-4235.
13. Evenepoel N, Agarwal P, Klein MT. Molecular-Level Kinetic Modeling of Lube Base Oil Hydroisomerization. *Energy & Fuels*.2018;32(9):9804-9812.
14. Froment GF. Single event kinetic modeling of complex catalytic processes. *Catalysis Reviews*.2005;47(1):83-124.
15. Standl S, Kirchberger FM, Kühlewind T, et al. Single-event kinetic model for methanol-to-olefins (MTO) over ZSM-5: Fundamental kinetics for the olefin co-feed reactivity. *Chemical Engineering Journal*.2020;402:126023.
16. Schweitzer J-M, Galtier P, Schweich D. A single events kinetic model for the hydrocracking of paraffins in a three-phase reactor. *Chemical Engineering Science*.1999;54(13-14):2441-2452.
17. Dewachtere NV, Santaella F, Froment GF. Application of a Single-Event Kinetic Model

- in the Simulation of an Industrial Riser Reactor for the Catalytic Cracking of Vacuum Gas Oil. *Chemical Engineering Science*.1999;54(15):3653-3660.
18. A CWG, A JWA, A WHG, B RHW. Reaction Mechanism Generator: Automatic construction of chemical kinetic mechanisms. *Computer Physics Communications*.2016;203:212-225.
 19. Van Geem KM, Reyniers M-F, Marin GB, Song J, Green WH, Matheu DM. Automatic reaction network generation using RMG for steam cracking of n-hexane. *AIChE Journal*.2006;52(2):718-730.
 20. Quann RJ, Jaffe SB. Building useful models of complex reaction systems in petroleum refining. *Chemical Engineering Science*.1996;51(10):1615-1635.
 21. Quann RJ, Jaffe SB. Structure-oriented lumping: describing the chemistry of complex hydrocarbon mixtures. *Industrial & Engineering Chemistry Research*.1992;31(11):2483-2497.
 22. Christensen G, Apelian MR, Hickey KJ, Jaffe SB. Future directions in modeling the FCC process: An emphasis on product quality. *Chemical Engineering Science*.1999;54(13):2753-2764.
 23. Chen J, Fang Z, Qiu T. Molecular reconstruction model based on structure oriented lumping and group contribution methods. *Chinese Journal of Chemical Engineering*.2018;26(8):1677-1683.
 24. Tian L, Shen B, Liu J. Building and Application of Delayed Coking Structure-Oriented Lumping Model. *Industrial & Engineering Chemistry Research*.2012;51(10):3923-3931.
 25. He G, Zhou C, Luo T, et al. Online Optimization of Fluid Catalytic Cracking Process via

- a Hybrid Model Based on Simplified Structure-Oriented Lumping and Case-Based Reasoning. *Industrial & Engineering Chemistry Research*.2020;60(1):412-424.
26. Peng B. *Molecular modelling of petroleum processes*, The University of Manchester; 1999.
 27. Feng S, Cui C, Li K, et al. Molecular composition modelling of petroleum fractions based on a hybrid structural unit and bond-electron matrix (SU-BEM) framework. *Chemical Engineering Science*.2019;201:145-156.
 28. Chen Z, Feng S, Zhang L, et al. Molecular-level kinetic modeling of heavy oil fluid catalytic cracking process based on hybrid structural unit and bond-electron matrix. *AIChE Journal*.2021;67(1):e17027.
 29. Guan D, Chen Z, Chen X, et al. Molecular-level heavy petroleum hydrotreating modeling and comparison with high-resolution mass spectrometry. *Fuel*.2021;297:120792.
 30. Chen Z, Feng S, Zhang L, et al. Molecular-level kinetic modelling of fluid catalytic cracking slurry oil hydrotreating. *Chemical Engineering Science*.2019;195:619-630.
 31. Chen Z, Yao X, Guan D, Zhao S, Zhang L, Xu C. Vacuum residue coking process simulation using molecular-level kinetic model coupled with vapor-liquid phase separation. *Chinese Journal of Chemical Engineering*.2022;41:301-310.
 32. John YM, Mustafa MA, Patel R, Mujtaba IM. Parameter estimation of a six-lump kinetic model of an industrial fluid catalytic cracking unit. *Fuel*.2019;235:1436-1454.
 33. Jacob SM, Gross B, Voltz SE, Weekman Jr VW. A lumping and reaction scheme for catalytic cracking. *AIChE Journal*.1976;22(4):701-713.
 34. Becker PJ, Celse B, Guillaume D, Dulot H, Costa V. Hydrotreatment modeling for a variety of VGO feedstocks: A continuous lumping approach. *Fuel*.2015;139:133-143.

35. Palos R, Rodríguez E, Gutiérrez A, Bilbao J, Arandes JM. Kinetic modeling for the catalytic cracking of tires pyrolysis oil. *Fuel*.2022;309:122055.
36. Qin X, Liu J, Wang C, et al. Molecular level analysis on performance of diameter expanding reactor to improve gasoline quality in FCC process. *Fuel*.2021;290:119978.
37. Chen Z, Sun N, Zhang L, Wang G, Zhao S, Gao J. Molecular-Level modeling for naphtha olefin reduction in FCC subsidiary Riser: From laboratory reactor to pilot plant. *Chemical Engineering Journal*.2022;437:135429.
38. Marin GB, Galvita VV, Yablonsky GS. Kinetics of chemical processes: From molecular to industrial scale. *Journal of Catalysis*.2021;404:745-759.
39. Xiong K, Lu C, Wang Z, Gao X. Quantitative correlations of cracking performance with physiochemical properties of FCC catalysts by a novel lump kinetic modelling method. *Fuel*.2015;161:113-119.
40. Quintana-Solórzano R, Rodríguez-Hernández A, García-de-León R. Study of the Performance of Catalysts for Catalytic Cracking by Applying a Lump-Based Kinetic Model. *Industrial & Engineering Chemistry Research*.2009;48(3):1163-1171.
41. Ravichander N, Chiranjeevi T, Gokak DT, Voolapalli RK, Choudary NV. FCC catalyst and additive evaluation—A case study. *Catalysis Today*.2009;141(1):115-119.
42. Vieira RC, Pinto JC, Biscaia EC, Baptista CMLA, Cerqueira HS. Simulation of Catalytic Cracking in a Fixed-Fluidized-Bed Unit. *Industrial & Engineering Chemistry Research*.2004;43(19):6027-6034.
43. Van Borm R, Reyniers M-F, Marin GB. Catalytic cracking of alkanes on FAU: Single-event microkinetic modeling including acidity descriptors. *AIChE*

- Journal*.2012;58(7):2202-2215.
44. Wang R, Li Y, Jiang G, et al. An efficient head-tail co-conversion process for high quality gasoline via rational catalytic cracking. *Chemical Engineering Journal*.2020;396:125210.
 45. Luo Y-R. *Comprehensive handbook of chemical bond energies*: CRC press; 2007.
 46. Corma A, Orchillés A. Current views on the mechanism of catalytic cracking. *Microporous and mesoporous materials*.2000;35:21-30.
 47. Yang M, Zhang L, Wang G, et al. Fischer-Tropsch wax catalytic cracking for the production of low olefin and high octane number gasoline: Experiment and molecular level kinetic modeling study. *Fuel*.2021;303:121226.
 48. Mochida I, Yoneda Y. Linear free energy relationships in heterogeneous catalysis: II. Dealkylation and isomerization reactions on various solid acid catalysts. *Journal of Catalysis*.1967;7(4):393-396.
 49. Evans MG, Polanyi MG. Some Applications of the Transition State Method to the Calculation of Reaction Velocities, Especially in Solution. *Transactions of the Faraday Society*.1935;31(6):1965-1967.
 50. Alvarez-Majmutov A, Chen J. Stochastic modeling and simulation approach for industrial fixed-bed hydrocrackers. *Industrial & Engineering Chemistry Research*.2017;56(24):6926-6938.
 51. Korre SC, Klein MT, Quann RJ. Polynuclear Aromatic Hydrocarbons Hydrogenation. 1. Experimental Reaction Pathways and Kinetics. *Industrial & Engineering Chemistry Research*.1995;34(1):101-117.
 52. Korre SC, Neurock M, Klein MT, Quann RJ. Hydrogenation of polynuclear aromatic

- hydrocarbons. 2. quantitative structure/reactivity correlations. *Chemical Engineering Science*.1994;49(24, Part A):4191-4210.
53. Cai G, Liu Z, Zhang L, Shi Q, Zhao S, Xu C. Systematic performance evaluation of gasoline molecules based on quantitative structure-property relationship models. *Chemical Engineering Science*.2021;229:116077.
54. Qu S, Liu G, Meng F, Wang L, Zhang X. Catalytic Cracking of Supercritical n-Dodecane over Wall-Coated HZSM-5 with Different Si/Al Ratios. *Energy & Fuels*.2011;25(7):2808-2814.
55. Tian Y, Liu H, Wang L, Zhang X, Liu G. Controllable fabrication and catalytic performance of nanosheet HZSM-5 films by vertical secondary growth. *AIChE Journal*.2018;64(6):1923-1927.
56. Corma A, Mengual J, Miguel PJ. Stabilization of ZSM-5 zeolite catalysts for steam catalytic cracking of naphtha for production of propene and ethene. *Applied Catalysis A: General*.2012;421:121-134.
57. Rahimi N, Karimzadeh R. Catalytic cracking of hydrocarbons over modified ZSM-5 zeolites to produce light olefins: A review. *Applied Catalysis A: General*.2011;398(1):1-17.
58. Rane N, Overweg AR, Kazansky VB, van Santen RA, Hensen EJM. Characterization and reactivity of Ga⁺ and GaO⁺ cations in zeolite ZSM-5. *Journal of Catalysis*.2006;239(2):478-485.